Vibronic Behavior and Electron Spin Relaxation of Jahn−Teller Complex $Cu(H_2O)_6^{2+}$ in $(NH_4)_2Mg(SO_4)_2 \cdot 6H_2O$ Single Crystal

Stanisław K. Hoffmann,* Janina Goslar, Wojciech Hilczer, Maria A. Augustyniak, and Miranda Marciniak

Institute of Molecular Physics, Polish Academy of Sciences, Smoluchowskiego 17, PL-60179 Poznañ, Poland

Received: June 4, 1997; In Final Form: December 4, 1997

Temperature dependences of the CW-EPR spectrum as well as the electron spin−lattice relaxation time T_1 and phase memory time T_M determined by electron spin echo were measured for Cu^{2+} ions in $(NH_4)_2Mg(SO_4)_2 \cdot 6H_2O$ single crystal. The dependences are dominated by vibronic behavior of the $Cu(H_2O)_6^{2+}$ complex and connected to the dynamic Jahn−Teller effect producing reorientations between two lowest energy wells of the adiabatic potential surface. Below 70 K the static Jahn−Teller effect is observed, and the system is strongly localized, by the local strains, in the deepest potential well leaving higher wells not populated. Above this temperature the second well becomes progressively populated, and a rapid averaging of the g_z and g_y factors as well as corresponding hyperfine splittings appears. The Boltzmann population of these two wells is achieved at 160 K. Simultaneously with g factors averaging a continuous broadening of the hyperfine lines is observed with line shape transformed from Gaussian at 70 K to Lorentzian at 160 K. The averaging and broadening processes are thermally activated with energy barrier $\delta_{12} = 108 \pm 3$ cm^{-1} = 156 K = 1.26 kJ/mol being the energy difference between the two deepest potential wells. Electron spin relaxation was measured below 50 K where electron spin-echo signal was detectable. Spin−lattice relaxation is driven by the direct and Raman processes with relaxation rate $1/T_1 = aT + bT^5$ as expected for dynamic Jahn−Teller systems. Spin−spin phase relaxation described by the phase memory time T_M depends on temperature as $1/T_M = a + bT + c \exp(-\Delta/kT)$ with $\Delta = 102 \pm 2$ cm^{-1}. At low temperatures the higher energy well is not populated; thus, Δ can be assigned as the energy of the first excited vibronic level in the deepest well. The Δ and δ_{12} are temperature-independent, indicating that adiabatic potential surface is not affected by temperature. We suggest that the deviations of experimental data from theoretically predicted vibronic g-factors averaging observed for Cu^{2+} in many Tutton salt type crystals are not due to temperature variations of the local strains or barrier height but are due to the fact that Boltzmann population of the potential wells cannot exist at low temperatures. This effect is especially pronounced for Cu^{2+} ions in $(NH_4)_2Mg(SO_4)_2 \cdot 6H_2O$ since the energy Δ of the first vibronic level is lower than the energy difference δ_{12} between adjacent wells. In such case the phonon-assisted tunneling jumps between the energy wells induced by two-phonon Raman processes via virtual state of energy δ_{12} become to be effective when $kT \geq \delta_{12}/2$, and the Boltzmann population of the second well is achieved via direct phonon process when thermal phonons of energy $kT \geq \delta_{12}$ are available.

1. Introduction

A constant interest in the Jahn−Teller type activity and vibronic coupling in solids is currently stimulated by searching of the high-temperature superconductivity mechanisms in copper(II) oxides[1] and dynamical bond deformation in fullerene molecules.[2] Moreover, still open questions exist in paramagnetic salts with Jahn−Teller active ions, particularly for Cu^{2+} in Tutton salt type crystals of general formula $M'_2M''(SO_4)_2 \cdot 6H_2O$ where M′ = NH_4, K, Rb, Cs, Tl and M″ = Cu, Zn, Cd, Mg, Co, Ni, Mn. The fluxional behavior of the $Cu(H_2O)_6^{2+}$ octahedra was observed by EPR both in copper(II)-doped diamagnetic Tutton salts[3−5] and in pure Cu(II) salts.[6−11] The molecular and crystal structure details and their temperature variations were studied in recent years with increasing accuracy by X-ray and neutron diffraction in hydrogeneous[12−14] and deuterated salts,[15−17] and a unified interpretation of the structural and fluxional behavior has recently been proposed.[18] The fluxional behavior is observed as temperature variation of the g-factors in EPR experiments. This is due to the temperature-dependent mixing of the d_{z^2} state into the ground state $d_{x^2-y^2}$ and is described currently by two models: a simple Silver−Getz (SG) model[3] and more general Riley−Hitchman (RH) model,[5,19] in terms of the intrawell and interwell dynamics of the three-well adiabatic potential surface. The form of the potential surface for an octahedral $Cu(H_2O)_6^{2+}$ complex results from a coupling between ^2E_g electron states and the Jahn−Teller-active ϵ_g normal vibration modes.[20] The displacements corresponding to the ϵ_g normal coordinates expressed in polar coordinates are

$$Q_\theta = \rho \cos \phi, \quad Q_\epsilon = \rho \sin \phi \tag{1}$$

where ρ is radial distortion parameter, and the ground-state wave function has the form

$$\psi_e = d_{x^2-y^2} \cos(\phi/2) + d_{z^2} \sin(\phi/2) \tag{2}$$

The vibronic Hamiltonian contains three terms:

* To whom correspondence should be addressed. E-mail skh@ifmpan.poznan.pl; fax (+48-61)86 84 524.

S1089-5639(97)01834-3 CCC: $15.00
Published on Web 02/14/1998

$$H_{\text{vibronic}} = H_0 + H_{\text{JT}} + H_{\text{strain}} \quad (3)$$

where H_0 is a pure vibrational term describing the undisturbed geometry with harmonic and anharmonic (K_3-term) contributions:

$$H_0 = [(\hbar\omega/2)(P_\theta^2 + P_\epsilon^2 + Q_\theta^2 + Q_\epsilon^2) + K_3 Q_\theta (Q_\theta^2 - 3Q_\epsilon^2)]I \quad (4)$$

where ω is the vibrational frequency, typically of the order 300 cm^{-1} in Tutton salts; P_i and Q_i are conjugate momenta and normal coordinates, respectively. K_3 is an anharmonicity constant, and I is the two-dimensional unit operator.

The Jahn−Teller Hamiltonian H_{JT} includes the first-order (linear) coupling A_1 and the second-order (nonlinear) coupling A_2:

$$H_{\text{JT}} = A_1(Q_\theta U_\theta - Q_\epsilon U_\epsilon) + A_2[(Q_\theta^2 - Q_\epsilon^2)U_\theta + 2Q_\theta Q_\epsilon U_\epsilon] \quad (5)$$

where U_θ and U_ϵ are pseudospin Pauli operators.

The $H_0 + H_{\text{JT}}$ Hamiltonian describes the shape of the potential energy surface in the Q_i-space. In harmonic approximation ($K_3 = 0$) with linear Jahn−Teller coupling ($A_2 = 0$) the potential surface has a well-known *Mexican hat* shape. At this level of approximation the Q_θ and Q_ϵ displacements are equivalent, and the energy minimum is a circular well of radius ρ. When higher order coupling terms are included, the perimeter of the *Mexican hat* becomes warped, giving three equivalent minima at $\phi = 0°$, 120°, and 240°. Thus, the *Mexican hat* potential contains three potential wells, each corresponding to a tetragonally elongated octahedral geometry with the $d_{x^2-y^2}$ ground state. The degree of warping, i.e., energy difference between the minima and saddle points, is equal to 2β, where $\beta \approx A_2\rho^2 \approx 20-350$ cm^{-1} in Tutton salts. In a low-symmetry environment the complex geometry is influenced additionally by lattice strains. These can be random strains (lattice defects) or nonrandom strains as chemical bonding, nonequivalent ligands, and packing effects. The strain effect can be parametrized in terms of the lattice strain components S_θ and S_ϵ in the Hamiltonian:

$$H_{\text{strain}} = S_\theta U_\theta - S_\epsilon U_\epsilon \quad (6)$$

where S_θ and S_ϵ are the tetragonal and orthorhombic strain components, respectively. The strains produce differences in the energy between potential wells. The strain effect can be especially large for dynamic Jahn−Teller systems with $\hbar\omega \gg 2\beta$ even at low temperatures and for small strain values. A distortion of the $Cu(H_2O)_6^{2+}$ complex from regular octahedron geometry is determined to a first approximation by the Jahn−Teller interaction, while the preferred direction of the distortion is dictated by the strain. Even a small strain will be vibronically enhanced and have a large effect on the complex geometry. The potential surface cross section along the Jahn−Teller perimeter deduced from neutron diffraction studies for $(NH_4)_2Cu(SO_4)_2{\cdot}6H_2O$ crystal[15] is shown in Figure 1 for tetragonal $S_\theta = -550$ cm^{-1} and orthorhombic $S_\epsilon = 120$ cm^{-1} strain parameters estimated from temperature variations of the Cu−O bond length. The axial strain component S_θ is negative, corresponding to a compression acting along the short Cu−O bond. The high-energy potential well 3 (Figure 1) is related to the shortest Cu−O(9) bond of the $Cu(H_2O)_6^{2+}$ which is not affected by temperature. The long and intermediate Cu−O bond lengths and corresponding EPR g_z and g_y factors vary with

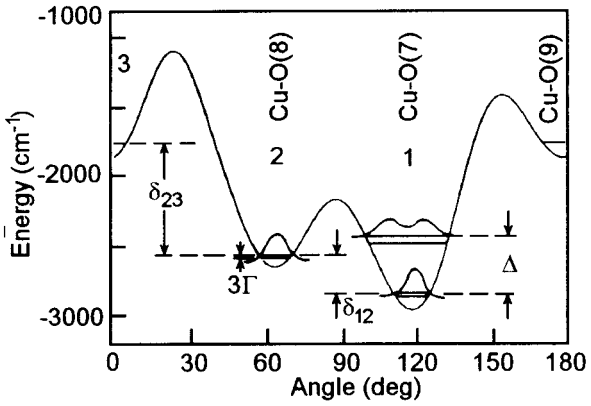

Figure 1. Adiabatic potential surface cross section along the Jahn−Teller perimeter calculated for the $(NH_4)_2Cu(SO_4)_2{\cdot}6H_2O$ single crystal with parameters[15] $\hbar\omega = 300$ cm^{-1}, $A_1 = 900$ cm^{-1}, $A_2 = 33$ cm^{-1}, $S_\theta = -550$ cm^{-1}, and $S_\epsilon = 120$ cm^{-1}.

temperature and depends on the energy difference between the two lower minima in the potential surface. This is decided largely by the orthorhombic S_ϵ component of the axial strain.

Silver and Getz,[3] in their model describing the g_z and g_y gradual coalescence on heating, assume that at 4 K all $Cu(H_2O)_6^{2+}$ complexes are elongated along z-axis direction i.e., Cu−O(7) bond. Thus, only well 1 is populated. As the temperature is raised, well 2, which is higher in energy of δ_{12}, becomes thermally populated. Simultaneously a fast relaxation, i.e., exchange between wells 1 and 2, appears which is faster than the splitting (in frequency units) between the respective EPR lines. As a result, the observed EPR spectrum is a population-weighted average of two spectra, and a continuous averaging of two higher molecular g-factors is observed on heating.

Riley and Hitchman have proposed a more general approach[5] assuming that the temperature g-factor averaging is due to a Boltzmann distribution over the vibronic levels. Each vibronic level has its own set of the g-factors, and a rapid relaxation gives an averaged g-factor. The SG model is a limiting case of the RH model corresponding to the one (or ocassionally two) vibronic level in the case of a strong vibronic wave function localization. This is approximately the case in Tutton salt crystals due to a large warping term in the vibronic Hamiltonian. Both models were successfully applied in describing the g-factors behavior both for copper(II) Tutton salt crystals and for Cu^{2+}-doped zinc(II) Tutton salts. The models assume that the adiabatic potential surface is temperature-independent. This assumption was questioned, and it was suggested that the lattice strains can vary with temperature,[18] producing variations in energy barrier between the wells.[10,11,21]

Except for a problem of validity of the above models, other effects and problems are currently studied and discussed in Tutton salt crystals. The question is a relationship between phenomenological lattice stress parameters S_θ and S_ϵ and interatomic or intermolecular interactions and lattice dynamics parameters. This problem is suggested by the fact that the direction of the largest $Cu(H_2O)_6^{2+}$ deformation in the rigid lattice limit is different for ammonium Tutton salts as compared to the other. Moreover, this direction can be switched to the second one by 1.5 kbar hydrostatic pressure or by deuteration of the crystal[12,15,17] which is correlated with changes in the hydrogen bond network between coordinated water molecules and SO_4^{2-} ions and associated with NH_4^+ ion reorientations.

The Jahn−Teller dynamics can be influenced by cooperative elastic coupling between Cu^{2+} ions. Effects such as an increase

in the barrier height, a change in the shape of the *g*-factor temperature dependence, an increase in the Jahn−Teller radius ρ, and change in the linear coupling coefficient A_1 in copper(II) Tutton salts as compared to the Cu^{2+}-doped diamagnetic salts were pointed out as a possible effects due to a cooperative coupling.[10,11,19] The cooperative elastic coupling can appear also in magnetically diluted systems, but the percolation threshold for an influence of the coupling on the Jahn−Teller dynamics in Tutton salts is not known, although our preliminary data suggest that it can be below of 1% of copper(II) concentration. This is in contradiction to the Jahn−Teller systems with the three-dimensional array of pulsating octahedra linked with each other by the common corners, where the threshold concentration of Cu^{2+} producing cooperative Jahn−Teller phase transition was found as $x = 0.23$ in $Ba_2Zn_{1-x}Cu_xO_6$,[22] as $x = 0.40$ in $K_2Zn_{1-x}Ca_xF_4$,[23] and as $x = 0.59$ in $Rb_2Mn_xMg_{1-x}F_4$[24] for the Jahn−Teller deformation ordering. The cooperative coupling in $(ND_4)_2Cu(SO_4)_2 \cdot 6H_2O$ can be responsible for the structural microdomains formation at low temperatures as reported from high-resolution X-ray diffraction studies.[14] On the other hand, it is well-known that superexchange coupling between Cu^{2+} ions in copper(II) Tutton salts is very small. This coupling is different in ammonium and potassium salts and seems to be dumped by Jahn−Teller dynamics of the $Cu(H_2O)_6^{2+}$ complexes.[9,11]

The above-described problems and questions show current fields of scientific activity in Jahn−Teller effect problems of Cu^{2+} ions in solids. Some of them, related to the Jahn−Teller dynamics, will be discussed in this paper for Cu^{2+} ions in $(NH_4)_2Mg(SO_4)_2 \cdot 6H_2O$ single crystal. This ammonium salt, which has the weaker hydrogen bonds between water molecules and SO_4^{2-} ions and stronger hydrogen bonding between NH_4^+ and SO_4^{2-} ions[25] than other diamagnetic Tutton salts, has been not studied in detail by EPR methods so far.

Information on the Jahn−Teller dynamics of the $Cu(H_2O)_6^{2+}$ complex in Tutton salt crystals was acquired mainly by CW-EPR and X-ray or neutron diffraction methods. It seems, however, that new data can be delivered by pulsed EPR methods which are sensitive to the individual spin packets forming inhomogeneously broadened EPR line. Because the spin packets are very narrow (10−100 μT), they are very sensitive to the lattice and molecular dynamics.

In this paper we present the spin−lattice and the spin−spin relaxation measurements by electron spin−echo technique. There are not many papers reporting electron spin-relaxation measurements in Jahn−Teller systems, and the available data were collected mostly at very low temperatures where relaxation rate is suffieciently low to be measured and where, unfortunately, the Jahn−Teller dynamics is very slow. The data are available mainly for spin−lattice relaxation time whereas the phase memory time T_M was studied in a few systems only, and its relation to the Jahn−Teller dynamics is unknown. This paper reports the first T_M measurements over a broad temperature range and its relation to the vibronic behavior of $Cu(H_2O)_6^{2+}$ complexes in solids. Three papers only report results of electron spin−lattice relaxation measurements in Tutton salt crystals. The direct spin−lattice relaxation process has been identified in $K_2Zn(SO_4)_2 \cdot 6H_2O:Cu^{2+}$ at liquid helium temperatures, and its magnetic field dependence was measured up to 1 T at 2.25 K.[26] A cross-relaxation between Cu^{2+} and Fe^{2+} ions has been studied by means of the CW-EPR line width changes in $(NH_4)_2Fe(SO_4)_2 \cdot 6H_2O$.[27] The crystals of $(NH_4)_2Mg(SO_4)_2 \cdot 6H_2O:Cu^{2+}$ were used as a model systems for introducing a new two-dimensional pulsed EPR technique known as electron-Zeeman-resolved EPR.[28] The temperature behavior of the phase memory time T_M has not been studied so far by pulsed EPR methods in Jahn−Teller crystals, and the existing data for Cu^{2+} in $ZnSiF_6 \cdot 6H_2O$ were obtained from the EPR line width temperature variations.[29]

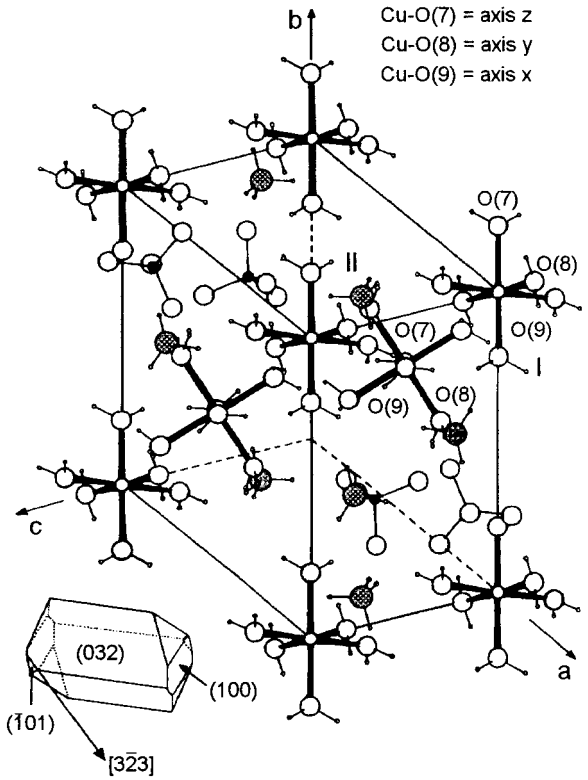

Figure 2. Projection of the $(NH_4)_2Cu(SO_4)_2 \cdot 6H_2O$ crystal unit cell along the [3$\bar{2}$3] direction and the crystal morphology. Copper(II) ions occupy two magnetically inequivalent sites I and II and deform the host complex with the **g**-tensor molecular axes: *x*, along Cu−O(9); *y*, along Cu−O(8); and *z*, along Cu−O(7), lying in the plane perpendicular to the [3$\bar{2}$3] direction.

2. Experimental Section

The single crystals were grown by slow evaporation at 300 K of a saturated aqueous solution of the stoichiometric amount of ammonium and magnesium sulfate with 0.1−2% of copper sulfate. The crystals grew in a form of elongated plates with well-developed (032) and (100) planes (Figure 2). The number of Cu^{2+} ions (unpaired spins) in the crystal was determined by an integration of the EPR spectra using $CuSO_4 \cdot 5H_2O$ single crystal as a spin standard. A linear relation between Cu^{2+} content in the mother solution and in the crystal was found with 2×10^{18} spins/g for 0.1% solution and 4×10^{19} spins/g for 2% solution.

Single-crystal EPR and ESE measurements were performed on a Bruker ESP380E FT/CW spectrometer with cylindrical dielectric TE_{011} cavity in the temperature range 4.2−300 K using flow helium Oxford CF935 cryostat. The temperature variations of the EPR spectra were recorded along the principal *g*-factor axes *x*, *y*, *z* at the selected rotational crystal orientation with the external magnetic field in the plane perpendicular to the [3$\bar{2}$3] direction. In this plane the **g**-tensor *z*-axis of the I-[$Cu(H_2O)_6$] complex and the *x*- and *y*-axis of the II-[$Cu(H_2O)_6$] complex are located, as presented in Figures 2 and 3. These two complexes arise from the two molecules related by 2-fold symmetry axis in the monoclinic unit cell of the crystal[15] with Cu(II) ions substituting the two Mg(II) sites. The EPR **g**-tensor

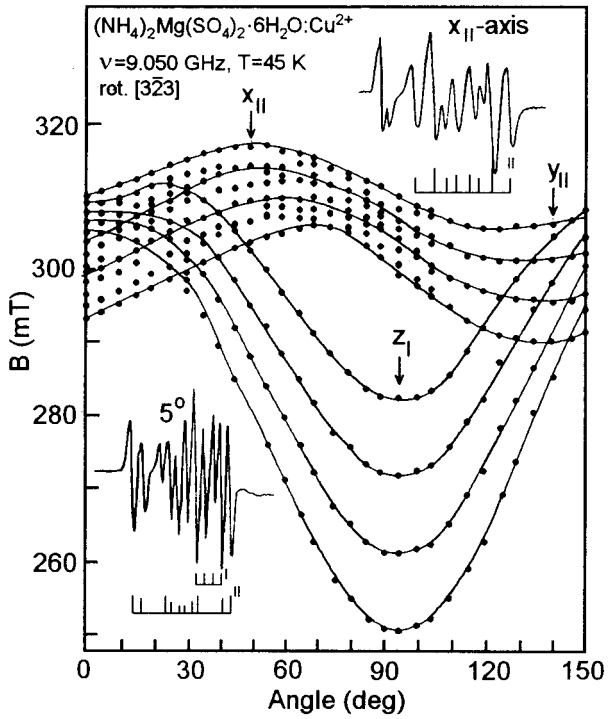

Figure 3. Angular variation of the EPR spectrum in the plane perpendicular to the [3$\bar{2}$3] direction at 45 K. The principal **g**-tensor axes are marked for two inequivalent copper(II) sites, i.e., the *z*-axis for complex I and the *x*- and *y*-axes for complex II. Two inserted spectra recorded at $\Theta = 5°$ and $\Theta = 50°$ and their stick diagrams show the main and the forbidden transition lines.

axes have different orientations for the both sites, producing two sets of hyperfine quartets in the most crystal orientations.

Pulsed EPR experiments were performed with magnetic field along *z*-axis direction where hyperfine lines from I-[$Cu(H_2O)_6$] sites are well-resolved. Spin−lattice relaxation time T_1 and phase memory time T_M were determined by the electron spin-echo (ESE) technique in the temperature range 4.2−50 K. Above 50 K the ESE amplitude was too low to be measured. The T_1 time was measured by the saturation recovery technique using a six 24 ns picket-fence saturation sequence. The single-exponential magnetization recovery was monitored by Hahn echo generated by two 24 ns pulses with 200 ns interpulse distance.

Phase relaxation described by the phase memory time T_M was measured as a decay of the Hahn echo generated by two 16 ns pulses vs interpulse distance. The initial interpulse distance was set to 96 ns. The decay was strongly modulated by a weak dipolar coupling between Cu^{2+} and surrounding magnetic nuclei: ^1H and ^{14}N. T_M was found to be independent of the pulse length up to 72 ns, indicating that the instantaneous diffusion contribution to the ESE decay is negligible.

The relaxation measurements were performed for the samples with the lowest spin concentration (0.1% in the solution) although a comparison with higher concentrations (1% in the solution) have not shown differences in T_1 and T_M values. It shows that the spectral diffusion within electron spin system is weak, and the spin relaxation is governed by coupling to the matrix nuclei. The measurements were performed for the four resolved hyperfine lines separately. The results have shown that the T_1 is the same for the all lines.

3. Results and Discussion

3.1. CW-EPR and Vibronic Effects. Angular variations of the single-crystal EPR spectra were recorded at room temperature, 120, 77, and 4.2 K by a rotation of a crystal around the [3$\bar{2}$3] direction in the microwave resonator. The rotational pattern is shown in Figure 3, where the principal *g*-factor directions x_{II}, y_{II}, and z_I for the two Cu^{2+} sites are marked and two spectra recorded at $\Theta = 5°$ and $\Theta = 50°$ are inserted. The hyperfine quartets are well-resolved in the spectra, and in the *xy*-plane they are strongly disturbed by the lines from forbidden transitions. The forbidden transition lines are comparable in intensity with the main transitions as can be seen from the stick diagram in Figure 3 and are due to a relatively strong quadrupole interaction of copper(II) nuclei with inhomogeneous electric crystal field. The quadrupole interaction is comparable with hyperfine splitting in the *xy*-plane as was discussed for Cu^{2+} in $(ND_4)_2Zn(SO_4)_2 \cdot 6H_2O$.[30]

Both the *g*-factors and hyperfine splittings *A* are temperature-dependent whereas the *x*, *y*, *z* axis directions are not. The rigid limit (4−60 K) spin-Hamiltonian parameters are in the range typical for Cu^{2+} ions in Tutton salt crystals:[4] $g_z = 2.432(2)$, $g_y = 2.105(2)$, $g_x = 2.079(2)$, $A_z = 120(2) \times 10^{-4}$ cm^{-1}, $A_y = 14(2) \times 10^{-4}$ cm^{-1}, $A_x = 37(3) \times 10^{-4}$ cm^{-1}. The solid lines in angular variations of Figure 3 are plotted with the above spin-Hamiltonian parameters.

The principal axis directions coincide with Cu−O bonds as is shown in Figure 2, and the maximal Jahn−Teller deformation of the $Cu(H_2O)_6^{2+}$ octahedron appears along the Cu−O(7) direction which is in contradiction to the non-ammonium Tutton salts where *z*-axis is along Cu−O(8) bond. This indicate that Cu^{2+} ions deform the host lattice structure to adopt the octahedron geometry typical for $(NH_4)_2Cu(SO_4) \cdot 6H_2O$.

Temperature variations of the *g*-factors and hyperfine splittings A_i are presented in Figure 4, a and b, respectively, and compared with Cu^{2+} data for analogous ammonium zinc(II) and cadmium(II) Tutton salts.[4,21]

The *g* factor averaging effect in our magnesium(II) salt appears in much narrower temperature range as compared to the other Tutton salts. The trace of the **g** and **A** tensors is weakly temperature dependent for Cu^{2+}in $(NH_4)_2Mg(SO_4)_2 \cdot 6H_2O$ with $g_z + g_y =$ constant and the small change in g_x. It suggests that the temperature variations are due to mainly to a dynamical averaging process.

This allows to apply the Silver−Getz model for a description of the $g(T)$ variations. This model assumes that the observed *g*-values are weighted averaged of the adiabatic potential well population:

$$g_z = \frac{N_1}{N} g_{z1} + \frac{N_2}{N} g_{y2} + \frac{N_3}{N} g_{x3}$$

$$g_y = \frac{N_1}{N} g_{y1} + \frac{N_2}{N} g_{z2} + \frac{N_3}{N} g_{y3} \qquad (7)$$

$$g_x = \frac{N_1}{N} g_{x1} + \frac{N_2}{N} g_{x2} + \frac{N_3}{N} g_{z3}$$

where $N = N_1 + N_2 + N_3$ and N_1, N_2, N_3 are the populations of the first, second, and the third well in Figure 1. The model assumes additionally that the magnetic parameters of the wells are identical. Neglecting the $g_x(T)$ variations ($N_3 = 0$) and taking $g_{z1} = 2.432$ and $g_{y1} = 2.106$ as the rigid limit values, the *g*-factor temperature variations can be calculated as

$$g_z(T) = N_1 g_{z1} + (1 - N_1) g_{y1} \qquad (8)$$

$$g_y(T) = N_1 g_{y1} + (1 - N_1) g_{z1}$$

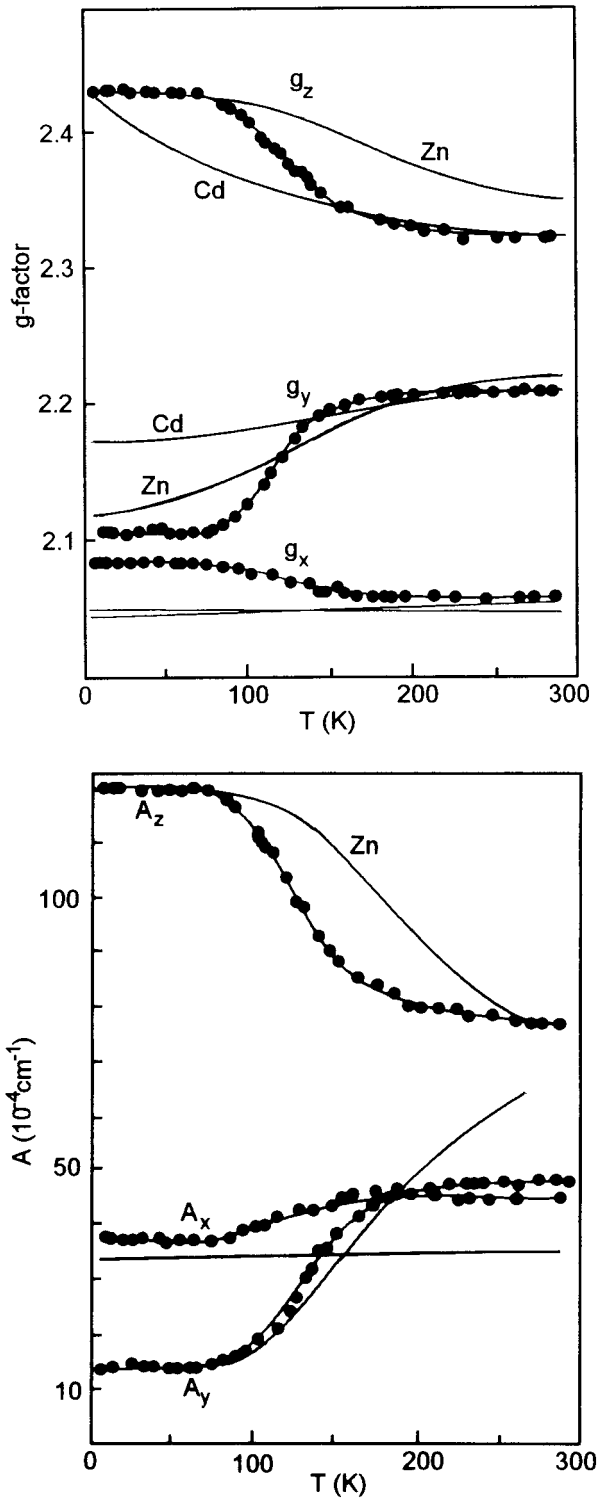

Figure 4. Temperature variations of the *g*-factors (a, top) and hyperfine splittings A_i (b, bottom) for copper(II) ion in ammonium Tutton salts: Mg(II), Zn(II),[4] and Cd(II).[21] Hyperfine splitting data for Cd(II) compound are not available.

This allows one to calculate the N_1 temperature dependence, and assuming a Boltzmann population of wells 1 and 2, i.e., $N_1/N_2 = \exp(\delta_{12}/kT)$ where $N_1 + N_2 = 1$, one can find the energy difference δ_{12} between the wells (see Figure 1) as a function of temperature. The result is shown in Figure 5 and compared with literature data for some other Tutton salt crystals. It is clearly seen that δ_{12} is not constant over the whole temperature range, indicating a restricted validity of the Silver−Getz model which is valid only when the δ_{12} splitting is

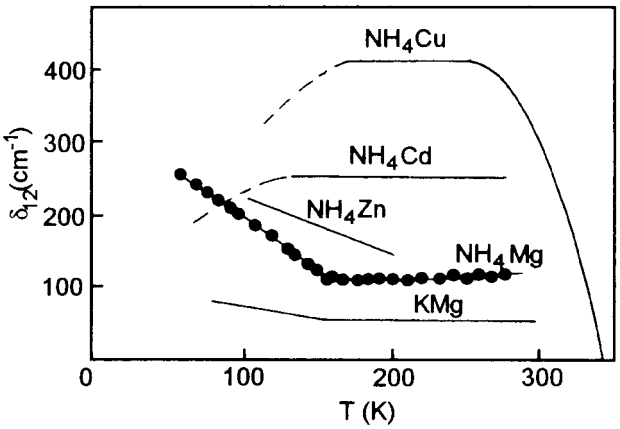

Figure 5. Temperature dependence of the energy difference δ_{12} between ground states of the potential wells 1 and 2 calculated using the Silver−Getz model[3] and experimental *g*-factor temperature variations for Cu^{2+} ions in Tutton salt crystals: $NH_4Mg = (NH_4)_2Mg(SO_4)_2 \cdot 6H_2O$, $NH_4Zn = (NH_4)_2Zn(SO_4)_2 \cdot 6H_2O$, $NH_4Cd = (NH_4)_2Cd(SO_4)_2 \cdot 6H_2O$,[21] $NH_4Cu = (NH_4)_2Cu(SO_4)_2 \cdot 6H_2O$,[11] and $KMg = K_2Mg(SO_4)_2 \cdot 6H_2O$.[31]

temperature-independent. The δ_{12} is higher for copper(II) Tutton salts as compared to the diamagnetic hosts (see data for $K_2Cu(SO_4) \cdot 6H_2O$ and $(NH_4)_2Cu(BeF_4)_2 \cdot 6H_2O$ crystals[11]), suggesting a cooperative elastic coupling between pulsating $Cu(H_2O)_6^{2+}$ octahedra. The δ_{12} is lower for non-ammonium salts as is seen for Cu^{2+} in $K_2Mg(SO_4)_2 \cdot 6H_2O$ crystal,[31] indicating an important role of the $SO_4 \cdots NH_4$ hydrogen bonds in determination of the adiabatic potential shape of admixtured Cu^{2+} complexes. The differences in δ_{12} for ammonium salts of Cd, Zn, and Mg, visible also clearly in *g*-factor temperature behavior (Figure 4a), reflect the slightly different adiabatic potential shape due to an adaptation of the strains by guest Cu^{2+} ions in the host lattice.

The δ_{12} in our crystal is practically temperature-independent above 160 K with $\delta_{12} = 108 \pm 3$ cm^{-1} = 156 K. The sharp change from $\delta_{12}(T)$ to δ_{12} = constant appears when $kT \approx \delta_{12}$. It means that at this critical temperature the thermal phonons appear with energy equal to the δ_{12}, allowing to keep thermal equilibrium between wells 1 and 2. It strongly suggests that below 160 K the Boltzmann population of the wells 1 and 2 does not exist. Assuming that δ_{12} is constant over the whole temperature range, we have calculated the population ratio N_2/N_1 predicted by the Silver−Getz model. The results of the calculations are compared with experimental data in Figure 6. It is clearly seen that indeed below 160 K the N_2/N_1 ratio is smaller than expected for the Boltzmann population of the wells. Moreover, below 70 K where *g*-factors are temperature-independent well 2 is not populated at all. Looking at the difference between theoretical line and experimental points at different temperatures, one can conclude that such effect cannot be explained as due to a continuous change of the adiabatic potential surface resulting from the lattice strain variations on heating. This conclusion is confirmed by pulsed EPR data described in the next sections. These data show that the activation energy of the vibronic motions is temperature-independent in this temperature range. So, we suppose that below 160 K that the mechanism which is able to keep the thermal equilibrium between distorted $Cu(H_2O)_6^{2+}$ configurations is not effective in our crystal. It seems that this conclusion is applied also for other Tutton salts (see Figure 5), but the effect is especially pronounced in $(NH_4)_2Mg(SO_4)_2 \cdot 6H_2O$ for a reason that will be more clear after presentation of electron phase relaxation measurements in the next section.

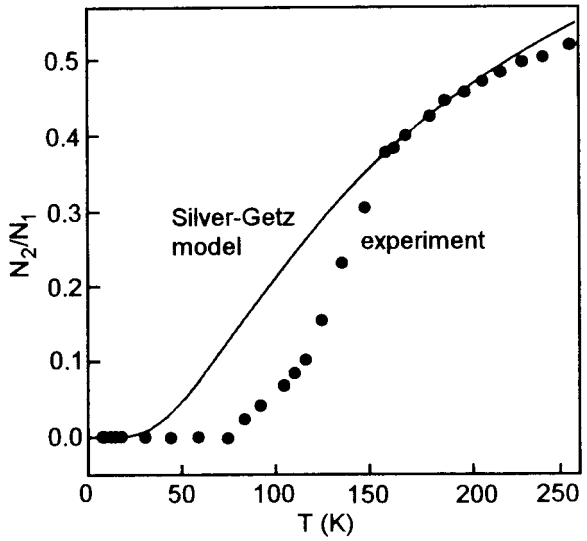

Figure 6. A comparison of the experimental population ratio N_2/N_1 of the two lowest potential wells (points) with that calculated from the SG model which assumes the Boltzmann population with $\delta_{12} = 108$ $cm^{-1} = 156$ K (solid line).

The conclusion that the population of the second potential well does not follow the Boltzmann law at low temperatures is not an easily accepted concept, and one should consider other possible explanation of this experimental result. One possible explanation is that at low temperatures the jumping rate between two potential wells is slow on the EPR time scale. If this rate is slower than the frequency difference between the EPR spectra of the two wells, the *g*-factor convergence will be not described by the SG model. In such case, however, the EPR spectra from the two wells should be simultaneously observed. It means that additional EPR lines from the complex located in the upper well should appear between two hyperfine quartets presented in Figure 3 at $\Theta = 95°$ (z_I-direction) in positions of y_{II}-lines approximately. Also the lines having z_I-positions and arising from the complex located in the upper well should appear at $\Theta = 140°$ (Figure 3). We have performed additional EPR measurements at temperature range 18−45 K looking for such lines which are expected to have rather small intensity as compared to the main lines from the lowest energy well. We have found no trace of such lines. It strongly suggests that the $Cu(H_2O)_6^{2+}$ complexes are localized in the deepest well at low temperatures. Such a possibility was suggested by Sturge on page 126 of his paper,[32] reporting vibronic dynamics of $Al_2O_3:Ni^{3+}$ system where he stated that when the energy difference δ_{12} between the potential wells is much lower that the tunneling splitting 3Γ, as is in our crystal, the thermal distribution among the wells will exists at temperatures such that $kT \geq \delta_{12}$.

In the same temperature range (70−160 K) where the rapid *g*-factors averaging appears, the strong and continuous broadening of the hyperfine lines is observed as presented in Figure 7 for $m_I = +1/2$ line along the *z*-axis of the complex I ($\Theta = 95°$, Figure 3). Simultaneously, the lines show a m_I dependence which is characteristic for the dynamic Jahn−Teller effect (see insets of Figure 7) and the line shape changes from Gaussian (below 76 K) to Lorentzian (above 160 K). Below 70 K there is no m_I variation of the line width and the interwell jumping can therefore be ruled out similarly as it was reported for Cu^{2+} in $K_2Zn(SO_4)_2 \cdot 6H_2O$.[3] For higher temperatures where *g*-factors are very weakly temperature-dependent the line width variations are very small, and moreover a broad background line appears, indicating an appearance of the spectrum with fully averaged

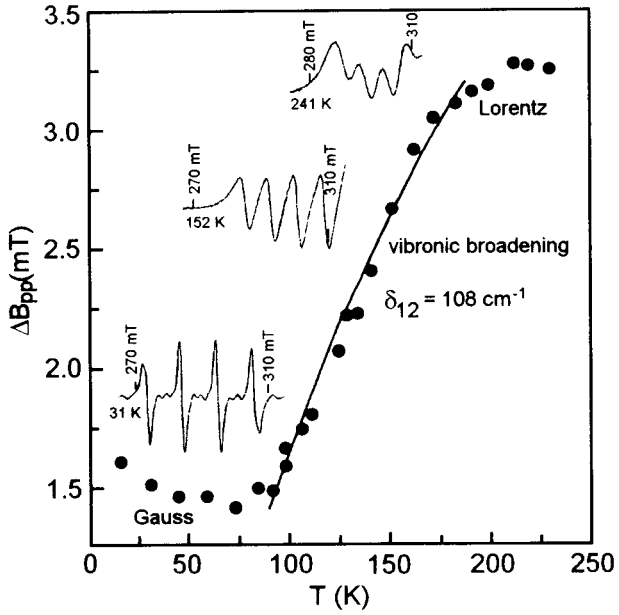

Figure 7. Temperature dependence of the peak-to-peak line width of the $m_I = +1/2$ hyperfine line of the complex I measured along the *z*-axis ($\Theta = 95°$ in Figure 3). The solid line presents the activation process described by the equation $\Delta B_{pp} = a + bT + c \exp(-\delta_{12}/T)$ with $a = 0.093$, $b = 0.000037$, $c = 6.7$, and the activation barrier $\delta_{12} = 156$ K $= 108$ cm^{-1}.

hyperfine splitting similarly to the effect observed for Cu^{2+} in $(NH_4)_2Cd(SO_4)_2 \cdot 6H_2O$.[21] The temperature dependence of the peak-to-peak line width ΔB_{pp} in the temperature range 70−160 K can be fitted to the equation $\Delta B_{pp} = a + bT + c \exp(-\delta_{12}/kT)$ with $\delta_{12} = 156$ K $= 108$ cm^{-1}, and the best fit is presented as a solid line in Figure 7. Thus, the line width is determined by the same thermally activated process as the vibronic *g*-factor averaging, i.e., the jumps of the $Cu(H_2O)_6^{2+}$ complex between two lowest energy distorted configurations 1 and 2 (Figure 1).

3.2. Electron Spin−Lattice Relaxation. Spin−lattice relaxation of Cu^{2+} ions in Jahn−Teller systems has been considered theoretically in a relation to the vibronic dynamics of the paramagnetic complex[32−35] although the experimental data for vibronic $Cu(H_2O)_6^{2+}$ complexes are available mainly for helium temperature region,[25,26,36] and only a few papers report the temperature variations of the spin−lattice relaxation time T_1 over a large temperature range.[29,37,38] The three mechanisms can contribute to the spin−lattice relaxation rate in Jahn−Teller systems: (i) Kramers−Van Vleck's mechanism within the ground-state doublet in each potential well which is typical for $S = 1/2$ ions without the Jahn−Teller effect. This effect is expected to contribute to the T_1 in very low-temperature range when Jahn−Teller dynamics is very slow;[4] (ii) A direct coupling via phonons between state of opposite spin in different distorted Jahn−Teller configurations being a consequence of the spin−orbit coupling to an excited state.[39] This Lee−Walsh mechanism can appear for static Jahn−Teller effect leading to the relaxation rate temperature dependence of the form $T_1^{-1} = aT + bT^3$ (for $kT > \delta_{12} > g\mu_B B$) with a and b coefficients depending on the δ_{12}/Δ_{cr} ratio, where Δ_{cr} is a crystal field splitting equal to $10Dq$. (iii) Reorientations (jumps) or tunneling between potential wells. This mechanism was found to dominate in most Jahn−Teller systems.

The possible reorientations over or through a potential barrier between adjacent potential wells as well as a phonon-induced tunneling have been already treated by quantum mechanical

theory.[40] When a system exhibits a static Jahn−Teller effect, the transitions between distorted configurations can be thermally activated. This may occur when the paramagnetic center absorbs a phonon and makes a real transition to one of the excited vibronic states. Then it can decay back to the ground state in a different distorted configuration. For real transitions to an excited state lying below the top of the barrier between the wells, the relaxation time τ for the recovery of the thermal equilibrium between the populations of the distorted configuration is

$$\tau^{-1} = \nu_0 \exp(-E/kT) \tag{9}$$

where the preexponential factor ν_0 is determined by the lifetime of the excited state and by the tunneling frequency ($3\Gamma/h$) through the barrier in the excited state, and E is the excitated vibronic state energy. For the levels lying above the barrier the τ^{-1} has the form (9) describing the classical jump rate with E being the barrier height and preexponential factor describing the classical oscillations in the well.

At lower temperatures, where thermal phonons of the energy E are not available, the phonon-assisted tunneling can dominate, which for $kT > \delta_{12}$ leads to the relaxation rate

$$\tau^{-1} = aT + bT^3 \int_0^{\Theta_D/T} \frac{x^2 \exp(x)}{[\exp(x) - 1]^2}\, dx \tag{10}$$

where the first term describes a direct transition accompanied by absorption of a single phonon (direct process) and the bT^3 term describes a two-phonon Raman process reduced by the transport integral I_2 which is dominant for $T \geq \Theta_D$. The a and b coefficients depend on the $(3\Gamma)^2$ where 3Γ is the tunneling splitting. When $\delta_{12} \approx kT$ and dynamical Jahn−Teller effect appears, the distorted configurations are mixed according to the Boltzmann population of the potential wells and the reorientation rate is

$$\tau^{-1} = aT + bT^5 \int_0^{\Theta_D/T} \frac{x^4 \exp(x)}{[\exp(x) - 1]^2}\, dx \tag{11}$$

where the terms describe the direct process linear with temperature and Raman processes reduced by I_4 transport integral, with a and b coefficients being dependent on δ_{12}.

The spin−lattice relaxation rate is slower than the reorientation rate τ^{-1} since only reorientations with the spin flip give contributions to the magnetic relaxation. The spin flips are possible due to the difference in anisotropy of the g-factor and hyperfine splitting for the different configurations. The spin−lattice relaxation time T_1 is proportional to τ by[35]

$$T_1^{-1} = \frac{2}{3}\left(\frac{\Delta g}{g} + \frac{\Delta A m}{h\nu}\right)^2 (\zeta_x^2\zeta_y^2 + \zeta_y^2\zeta_z^2 + \zeta_z^2\zeta_x^2)\tau^{-1} \tag{12}$$

where ζ_i are the direction cosines of the magnetic field with respect to the distortion axis.

Thus, the general expression for the temperature dependence of the spin−lattice relaxation rate of the Jahn−Teller active paramagnetic center is

$$T_1^{-1} = aT + bT^3 I_2 + cT^5 I_4 + d \exp(-E/kT) \tag{13}$$

The results of our T_1^{-1} measurements in the temperature range 4.2−55 K presented in a log−log scale in Figure 8 clearly show that the spin−lattice relaxation is due to the direct and Raman processes and described by the equation

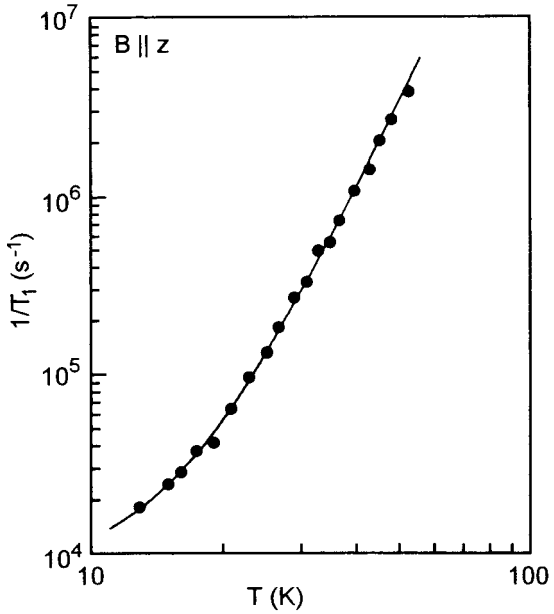

Figure 8. Temperature dependence of the spin−lattice relaxation rate. The solid line is a plot of the equation $T_1^{-1} = 1100T + 0.0105T^5$.

$$T_1^{-1}\,(s^{-1}) = 1100T + 0.0105T^5 \tag{14}$$

The solid line in Figure 8 is plotted according to eq 14.

The similar temperature behavior of T_1 was found for Cu^{2+} in $La_2Mg_3(NO_3)_{12} \cdot 24H_2O$,[37] whereas the $T_1^{-1} = aT + bT^3$ dependence was reported for Cu^{2+} in $ZnSiF_6 \cdot 6H_2O$.[29] The Orbach-type $\exp(-E/kT)$ relaxation was observed for Cu^{2+} in $Zn(BrO_3)_2 \cdot 6H_2O$,[36] although the $T_1^{-1} \propto T^3$ dependence was reported for this crystal also.[37] In the all of the above crystals and for Cu^{2+} in $(NH_4)_2Mg(SO_4)_2 \cdot 6H_2O$ the T_1 values in the temperature range 4.2−10 K are of the order of $T_1 = 10^{-4}$ s. This is shorter but not significantly than T_1 for Cu^{2+} in crystals without Jahn−Teller effect, e.g., $T_1 = 3 \times 10^{-4}$ s for Cu^{2+} in triglycine selenate at 10 K,[41] $T_1 = 1 \times 10^{-2}$ s for Cu^{2+} in Ni bis(diethyldithiocarbamate) at 10 K,[42] and $T_1 = 5 \times 10^{-2}$ s for Cu^{2+} in $LiNbO_3$ at 10 K.[43] To have a direct proof that Jahn−Teller dynamics governs the spin relaxation in our crystal, we have measured T_1 for Mn^{2+} ions in $(NH_4)_2Mg(SO_4)_2 \cdot 6H_2O$ along the z-axis direction of the Cu^{2+} complex, and we found that at 10 K the $T_1(Mn^{2+}) = 1 \times 10^{-2}$ s.[44] The Mn^{2+} is not a Jahn−Teller ion, and its relaxation in the same host lattice is of about 2 orders of magnitude slower than Cu^{2+}, indicating a dominat role of the Jahn−Teller dynamics in electron spin relaxation.

3.3. Phase Spin−Spin Relaxation. The phase relaxation, i.e., a decay of the transversal magnetization, can be measured by the electron spin-echo (ESE) technique. Results of such measurements are available only for $Cu(H_2O)_6^{2+}$ in $La_2Mg_3(NO_3)_{12} \cdot 24H_2O$ in the temperature range 2−10 K.[37] The modulated single-exponential ESE amplitude decay was observed with temperature dependence of the phase memory time governed by direct process only, i.e. $T_M^{-1}\,(s^{-1}) = 1.5 \times 10^5 + 8.25 \times 10^4 T$.

In $(NH_4)_2Mg(SO_4)_2 \cdot 6H_2O$:$Cu^{2+}$ single crystals we were able to detect the ESE signal up to about 53 K. At a given temperature the two-pulse ESE amplitude decreases when interpulse distance τ_p increases. It is due to spin and/or spectral diffusion processes producing random changes of the precession phase of the excited spins of the spin packets forming an

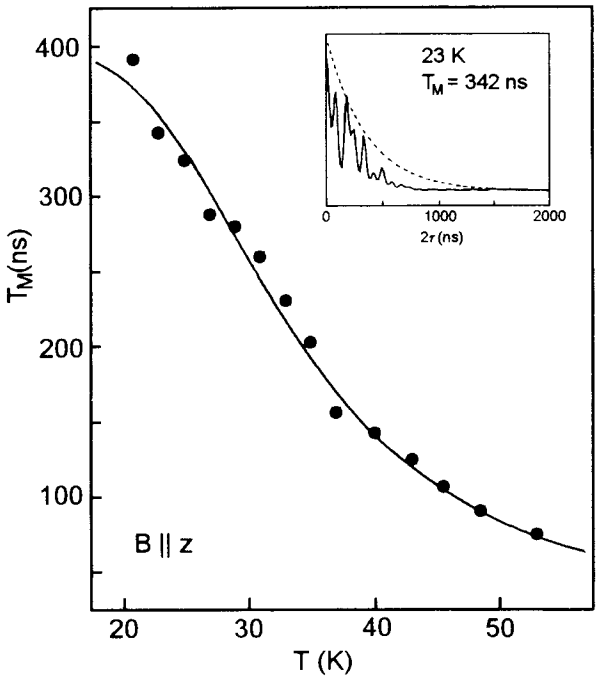

Figure 9. Temperature variation of the phase memory time T_M. The solid line is the best fit to the equation $1/T_M = a + bT + c \exp(-\Delta/kT)$ with $\Delta = 102$ cm^{-1}. The inset shows the modulated decay of the ESE amplitude at 23 K approximated by single-exponential function with $T_M = 342$ ns.

inhomogeneously broadened EPR line. An exponential decay of the ESE amplitude $V(t)$ can be described by the function

$$V(t) = V_0 \exp(-t/T_M), \quad t = 2\tau_p \tag{15}$$

The characteristic time T_M is called the phase memory time, and describing the width of the spin packet $T_M = 1/\Delta B_{packet}$, whereas the shape of the spin packet is given by the Fourier transform of the decay function $V(t)$. The ESE decay in our crystal was strongly modulated by a weak dipolar coupling of Cu^{2+} to surrounding proton ^{1}H and nitrogen ^{14}N nuclei as is shown in the inset of Figure 9. The decay was approximated by eq 15 (dashed line in the inset of Figure 9), and the temperature variation of T_M is presented in Figure 9.

T_M strongly decreases on heating, indicating a continuous spin packet broadening from 14 μT at 20 K to 71 μT at 53 K. It means that the EPR line becomes more homogeneous and as a result the ESE amplitude diminishes on heating, and above 55 K the ESE signal is nondetectable. The temperature dependence of T_M was fitted to the equation

$$T_M^{-1}\,(\mathrm{s}^{-1}) = 2.5 \times 10^6 + 1.0 \times 10^3 T + 1.8 \times 10^8 \exp(-\Delta/kT) \tag{16}$$

where $\Delta = 102 \pm 2$ cm^{-1}, and the best fit is presented by the solid line in Figure 9.

There is no theory of the electron phase relaxation in the Jahn−Teller systems although there exist the theories for the systems without the Jahn−Teller effect. These theories predict that for sufficiently low Cu^{2+} ion concentration the spectral diffusion within the unpaired electrons system can be negligible, and then the phase relaxation is governed by nuclear spectral diffusion, i.e., random fluctuations of the local dipolar field produced by the matrix nuclei and modulated by paramagnetic center and/or molecular motions.[45,46] This is the case in our crystal.

The data presented in Figure 9 suggest that the decrease of T_M on heating is related to the spin packet broadening effect due to the dynamics of the $Cu(H_2O)_6^{2+}$ complexes. An exponential term in eq 16 indicates that this is an activation process with activation energy $\Delta = 102$ cm^{-1}, which lies in the range of the vibronic level splitting for Cu^{2+} in Tutton salt crystals (see Figure 1). Thus, it seems that spin phase relaxation of Cu^{2+} in $(NH_4)_2Mg(SO_4)_2 \cdot 6H_2O$ is governed by excitation to a higher vibronic level and decay back, since the population of well 2 is negligible at low temperatures and no jumps between wells 1 and 2 exist as was discussed in section 3.1. Such a mechanism of the phase relaxation seems to be possible due to the electronic part of the vibronic wave function and is not efficient for pure vibrational excitations. Equation 16 shows that at low temperatures the contribution from direct phonon process dominates, whereas for higher temperatures T_M is dominated by thermally activated process between vibronic levels in the same well.

The phase relaxation measurements show a high sensitivity of T_M to the vibronic dynamics. Because of very narrow spin packets, the T_M shortening can be observed at very low temperatures where CW-EPR spectra are not sensitive yet.

3.4. The Barrier, Reorientations, and Spin−Spin Relaxation. The Jahn−Teller effect of $Cu(H_2O)_6^{2+}$ octahedrons in Tutton salts is classified as a strong effect. It means that the Jahn−Teller stabilization energy $E_{JT} = A_1^2/(2h\nu)$ is large as compared to the vibronic energy and can be evaluated from the data of ref 5 as of about 1350 cm^{-1}. The warping 2β of the *Mexican hat* potential surface is also relatively large with $\beta = A_2A_1^2/(h\nu)^2 = 300$ cm^{-1}; thus, the potential wells are rather deep. Due to the strong Jahn−Teller effect, the splitting between vibronic levels is large and tunneling splitting 3Γ is small and can be evaluated from the β-value[34] as $3\Gamma \approx 0.5$ cm^{-1}, which is comparable to the $3\Gamma \geq 0.3$ cm^{-1} of $Cu(H_2O)_6^{2+}$ in $La_2Mg_3(NO_3)_{12} \cdot 2H_2O$[33] and Ni^{3+} in Al_2O_3 ($3\Gamma \approx 1$ cm^{-1}).[32,34] However, the dynamic Jahn−Teller effect for Cu^{2+} in Tutton salt crystals is dominated by the strains which can be identified as the hydrogen bonds between coordinated water molecules and surrounding SO_4 molecules. The strains produce an inequivalence of the three potential wells. The population of the two lowest energy wells, differ in energy of δ_{12} (Figure 1), allows to explain the experimentally observed effects.

We found, as described above, that the phase spin−spin relaxation, hyperfine line width, and the g-factor temperature variations are thermally activated processes.

Phase memory time T_M is determined mainly by the transitions to the excited vibronic level of energy $\Delta = 102$ cm^{-1} (Figure 9). The continuous increase in the phase relaxation rate $1/T_M$ on heating reflects a continuous spin packet broadening. Thus, one can expect the resonance line becomes homogeneously broadened at some temperature; i.e., it will be formed from a single spin packet. The width of such a line can be described by the effective spin−spin relaxation time $T_2^* \propto 1/\Delta B_{pp}$, and the line should be continuously broadened, reflecting spin packet behavior when temperature increases. It is indeed observed in the temperature range 70−160 K (Figure 7), where the line shape continuously changes from Gaussian to Lorentzian. For the Lorentzian line the relation between T_2^* and ΔB_{pp} is

$$T_2^*\,[\mathrm{s}] = \frac{13.1306}{g\Delta B_{pp}\,[\mathrm{mT}]} \times 10^{-9} \tag{17}$$

The calculated $1/T_2^*$ from data of the Figure 7 are compared with $1/T_M$ in Figure 10. Both the $1/T_2^*$ and $1/T_M$ temperature

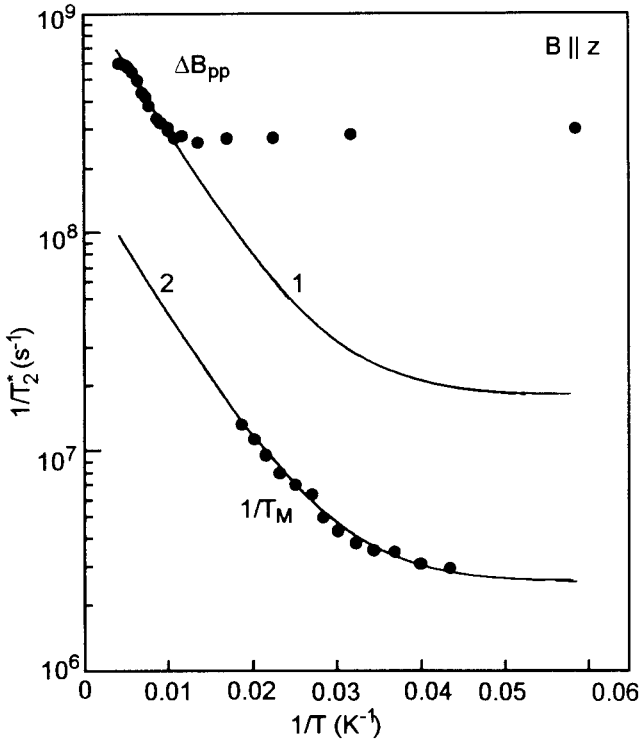

Figure 10. A log−log plot of the effective spin−spin relaxation rate $1/T_2^*$ vs reciprocal temperature calculated from the hyperfine ($m_I = +1/2$) line width (Figure 7) at high temperatures and equal to the $1/T_M$ at lower temperatures. The solid curves are the best fits to the equation $1/T_2^* = a + bT + c\exp(-E/kT)$ with (1) $a = 17.4 \times 10^6\ s^{-1}$, $b = 6928\ s^{-1}\ K^{-1}$, $c = 12.4 \times 10^8\ s^{-1}$, $E = \delta_{12} = 108\ cm^{-1}$ and (2) $a = 2.5 \times 10^6\ s^{-1}$, $b = 1000\ s^{-1}\ K^{-1}$, $c = 1.8 \times 10^8\ s^{-1}$, $E = \Delta = 102\ cm^{-1}$. Curves 1 and 2 are shown also in Figure 7 and Figure 9.

variations can be fitted to the same equation $(T_2^*)^{-1} = a + bT + c\exp(-E/kT)$ with different a, b, and c and $E = \delta_{12}$ for the line width $1/T_2^*$ and $E = \Delta$ for the phase relaxation. $1/T_2^*$ is larger than $1/T_M$, indicating that phase relaxation is only one of the contributions to the total line width ΔB_{pp} which can be written as

$$\Delta B_{pp} \propto \Delta B_{pp}^0 + \frac{1}{T_M} + \frac{1}{2T_1} \qquad (18)$$

The first term is a background line width and can be due to not complete homogeneity of the line. The last term is due to the spin−lattice relaxation contribution which becomes comparable to the T_M contribution close to 100 K. Thus, only a part of the resonance line is determined by spin-relaxation processes, and this contribution can be related to the vibronic dynamics and reorientations between distorted Jahn−Teller configurations. The total line width can be, in principle, calculated using more sophisticated theories of the magnetic relaxation in Jahn−Teller systems.[47] The above comparison between the line width and the relaxation times clearly indicates that there exists a relation between these parameters, but this is not a direct proportionality. So, an evaluation of the T_1 or T_M from the line width behavior at higher temperatures, which is commonly use in EPR experiments, as for example for Cu^{2+} in $ZnSiF_6 \cdot 6H_2O$,[29] seems to have a restricted validity.

In $(NH_4)_2Mg(SO_4)_2 \cdot 6H_2O$ crystal, the difference between energy Δ determined from $T_M(T)$ and δ_{12} determined from the SG model of g-factor vibronic behavior and $\Delta B_{pp}(T)$ is rather small but seems to be essential. The Δ and δ_{12} for $Cu(H_2O)_6^{2+}$ in different Tutton salts are summarized in Table 1. In contrast

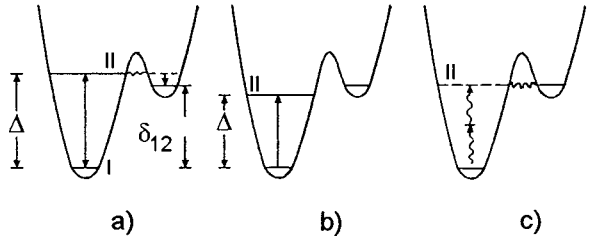

Figure 11. Three mechanisms of interwell transitions when tunneling splitting is very small ($3\Gamma \ll \delta_{12}$): (a) phonon-controlled tunneling from the excited vibronic state, (b) no tunneling is possible from the excited state, (c) the two-phonon Raman process−phonon assited tunneling mechanism.

TABLE 1: Energy of the First and Second Vibronic States (in cm^{-1}) of the $Cu(H_2O)_6^{2+}$ Vibronic Complex in Tutton Salts $A_2M(SO_4)_2 \cdot 6H_2O$

A_2M	K_2Zn	Rb_2Zn	NH_4Zn	Cs_2Zn	NH_4Mg
δ_{12}	75 (72)	153	181	235	108
D	120 (187)	216	235	292	102
ref	3 (5)	5	5	5	this paper

to the other salts where $\Delta > \delta_{12}$ we found $\Delta < \delta_{12}$ for Cu^{2+} in $(NH_4)_2Mg(SO_4)_2 \cdot 6H_2O$. This seems to be the main reason of difference in vibronic g-factors behavior in magnesium(II) salts and the other Tutton salt crystals and can be understood looking on possible excitations in an asymmetrical double-well potential for the case of a low tunneling probabillity between the vibronic ground states as discussed below.

Our experiments show a non-Boltzmann population of the potential energy wells at low temperatures but a Boltzmann population of the vibronic levels in the deepest well. It means that the excited vibronic levels of the deepest well become progressively thermally populated as temperature raises, but simultaneously the mechanisms that can allow to jump the $Cu(H_2O)_6^{2+}$ complex to the second well are not effective at low temperatures. These mechanisms can be related to the interwell tunneling or to the real jumps over the barrier. The overbarrier jumps are not probable at low temperatures because the barrier is very high in Tutton salts, owing the large value of the warping term in the vibronic Hamiltonian. The direct tunneling between the ground states of the adjacent wells does not exist since the tunneling splitting 3Γ is very small as compared to the energy difference δ_{12} between the wells: 3Γ ($0.5\ cm^{-1}$) $\ll \delta_{12}$ ($108\ cm^{-1}$). But tunneling processes are still possible via excited states lying close to the barrier top. The processes can occur via real excited vibronic state of energy Δ and are called *the phonon-controlled tunneling* or, via a virtual energy level, *the phonon-assisted (induced) tunneling.*[3,40] These processes are schematically shown in Figure 11. The phonon-controlled tunneling is possible when $\Delta \geq \delta_{12}$ as shown in Figure 11a. The excited vibronic level II is thermally populated. From this excited state the system can tunnel to the second well and then decay to the ground state of this well. The Boltzmann population of the second well is kept over the whole temperature range. When $\Delta < \delta_{12}$ (Figure 11b), however, no tunneling is possible from the excited state II into the second well. So, although the level II has Boltzmann population, the second well is not populated at all up to the temperature where $kT \geq \delta_{12}$. It seems that this is the case suggested by Sturge.[32] Such a situation we found in our crystal, and a similar situation can be expected for Cu^{2+} in $CsZn(SO_4)_2 \cdot 6H_2O$ as suggested by Figure 3 of Hitchman's paper.[5]

The thermal population of the both wells can be kept even when no thermally accessible vibronic state exists. It can be done by phonon-induced transitions via a virtual energy level

when the direct and/or Raman phonon processes are effective. The direct phonon excitation to the virtual state II of energy E and subsequent tunneling to the second well appears when $E \geq \delta_{12}$ i.e., for $T \geq 156$ K where thermal phonons of energy E are available. The two-phonon Raman processes begin to be effective in population of the second well when $kT \geq \delta_{12}/2$ as shown in Figure 11c, i.e., for $T \geq 78$ K where two phonons of energy $\delta_{12}/2$ can put together producing the excited virtual state of energy δ_{12}. These two critical temperatures can be clearly recognized in Figure 6 where the population of the second well starts at $T > 70$ K and the Boltzmann population is reached at about 160 K. The higher order Raman processes as well as the direct and Raman processes in excited vibronic state II (Figure 11b) are not effective as is indicated by our experimental data.

4. Conclusions

Dynamic behavior of $Cu(H_2O)_6^{2+}$ complexes in the $(NH_4)_2Mg(SO_4)_2 \cdot 6H_2O$ lattice can be explained by taking into account the vibronic energy levels and their thermal population in the two lowest wells 1 and 2 (Figure 1) of the adiabatic potential surface, similarly to Cu^{2+} in other Tutton salt type crystals. Existing models of the vibronic $Cu(H_2O)_6^{2+}$ dynamics are based on the experimentally determined temperature variations of the g-factors and line width of the Cu^{2+} EPR spectra and X-ray and neutron diffraction studies. We found that an additional and very essential piece of information is supplied by the temperature dependence of the electron phase relaxation studied by electron spin echo (ESE). The EPR and ESE temperature variations can be divided into three distinct regions:

Below 70 K. The $Cu(H_2O)_6^{2+}$ complexes are strongly localized in the deepest potential well (well 1) by the local strains with a strong static Jahn−Teller effect. The upper well 2 is not populated. The EPR parameters are temperature-independent, and the individual hyperfine lines are inhomogeneously broadened with the Gaussian shape, and there is no m_I dependence of the line width. The phase memory time, however, strongly decreases on heating in this rigid lattice limit, and its temperature dependence indicates that the phase relaxation process is due to the thermally (phonon) activated excitations to the state with energy $\Delta = 102$ cm^{-1} (1.20 kcal/mol) with Δ being temperature independent. Since the well 2 is not populated in this temperature range, Δ has thus to be considered as the energy of the first excited vibronic level in well 1.

In the Temperature Range 70−160 K. The first excited $Cu(H_2O)_6^{2+}$ configuration, i.e., well 2, is rapidly populated on heating, but the Boltzmann population of wells 1 and 2 is not achieved up to 160 K where the thermal phonons' energy kT reaches energy δ_{12} of the ground state in well 2. The most dramatic changes in EPR spectrum are observed in this temperature range. The g_z and g_y factors as well as A_z and A_y hyperfine splittings are averaged with simultaneous line broadening and $\Delta B_{pp}(m_I)$ dependence characteristic for a dynamic Jahn−Teller effect, i.e., jumps between distorted Jahn−Teller configurations (potential wells) 1 and 2. The averaging and broadening are thermally activated with identical activation energy $\delta_{12} = 108$ cm^{-1} (1.26 kJ/mol) (see Figure 1). The line shape is continuously transformed from Gaussian to Lorentzian, and at about 160 K hyperfine lines are practically homogeneously broadened. Because of this and the fast spin relaxation, the ESE signal disappears, and neither spin−lattice nor phase relaxation can be measured.

Above 160 K. Wells 1 and 2 are thermally populated according to the Boltzmann law, and g-factors are continuously but slowly averaged according to the Silver−Getz model with the energy difference $\delta_{12} = 108$ cm^{-1}. The EPR lines are Lorentzian and homogeneously broadened.

Both the vibronic level splitting in the low-temeperature range and the barrier height in the higher temperature range are temperature-independent, indicating that the adiabatic potential surface is not affected by temperature in the whole temperature range. Thus, according to our data, the previously observed deviations between theoretical predictions and experiments explained tentatively as a result of the temperature dependence of the local strains or/and the barrier height[10,11,18,21] can have different interpretations. The adiabatic potential surface determined by Jahn−Teller and strain forces is stable, but the Boltzmann population of the potential wells does not exist in the whole temperature range and can appear only above the temperature where the thermal phonons have energy larger than the barrier height. This effect is especially pronounced for Cu^{2+} in $(NH_4)_2Mg(SO_4)_2 \cdot 6H_2O$ where the most rapid g-factor vibronic averaging appears in a relatively narrow temperature range in contrast to the other Tutton type salt crystals. Such behavior we relate to the opposite sequence of Δ and δ_{12} in $(NH_4)_2Mg(SO_4)_2 \cdot 6H_2O$, i.e., $\Delta \leq \delta_{12}$ as compared to the $Cu(H_2O)_6^{2+}$ in other Tutton salt crystals where $\Delta > \delta_{12}$ (see Table 1).

The spin−lattice relaxation exhibits the temperature variation $1/T_1 \propto T^5$ characteristic for the dynamic Jahn−Teller effect. The question is, however, why there is no contribution from the Orbach−Aminov process via the excited vibronic state of energy Δ which is so effective in the phase relaxation. Probably the excitations to, and relaxation back from, this level are realized without spin flip or the temperature range for T_1 measurements by the electron spin-echo technique is too narrow (50 K only) to detect all spin−lattice relaxation processes. On the other hand, the question is why the Raman processes are effective in spin−lattice relaxation but not in transitions between the wells. It seems to be due to the fact that the Zeeman energy is of the order of 0.3 cm^{-1} whereas the interwell energy is $\delta_{12} = 108$ cm^{-1}.

Acknowledgment. This work was supported by the Polish Scientific Research Committee under Project KBN-2-P03B-038-08. The authors gratefully acknowledge the technical assistance of M. Sc. M. Gramza and M. Sc. P. Morawski.

References and Notes

(1) Fil, D. V.; Tokar, O. I.; Shelankov, A. L.; Weber, W. *Phys. Rev. B* **1992**, *45*, 5633.
(2) Tosatti, E.; Manini, N.; Gunnarsson, O. *Phys. Rev. B* **1996**, *54*, 17184.
(3) Silver, B. L.; Getz, D. *J. Chem. Phys.* **1974**, *61*, 638.
(4) Petrashen, V. E.; Yablokov, Yu. V.; Davidovitch, R. L. *Phys. Status Solidi B* **1980**, *101*, 117.
(5) Riley, M. J.; Hitchman, M. A.; Mohammed, A. W. *J. Chem. Phys.* **1987**, *87*, 3766.
(6) Waite, T. D.; Hitchman, M. A. *Inorg. Chem.* **1976**, *15*, 2155.
(7) Hitchman, M. A. *J. Chem. Phys.* **1978**, *68*, 3425.
(8) Alcook, N. W.; Duggan, M.; Murray, A.; Tyagi, S.; Hathaway, B. J.; Hewat, A. *J. Chem. Soc., Dalton Trans.* **1984**, 7.
(9) Hoffmann, S. K.; Gomółka-Marciniak, M. *Solid State Commun.* **1993**, *86*, 63.
(10) Hoffmann, S. K.; Gomółka-Marciniak, M. *Acta Phys. Polon. A* **1993**, *83*, 817.
(11) Marciniak, M.; Hoffmann, S. K.; Augustyniak, M. A.; Hilczer, W. *Phys. Status Solidi B* **1995**, *191*, 201.
(12) Hathaway, B. J.; Hewat, A. W. *J. Solid State Chem.* **1984**, *51*, 364.
(13) Figgis, B. N.; Iversen, B. B.; Larsen, F. K.; Reynolds, P. A. *Acta Crystallogr.* **1993**, *B49*, 794.
(14) Figgis, B. N.; Reynolds, P. A.; Hanson, J. C.; Mutikainen, I. *Phys. Rev. B* **1993**, *48*, 13372.
(15) Simmons, C. J.; Hitchman, M. A.; Stratemeier, H.; Schultz, A. J. *J. Am. Chem. Soc.* **1993**, *115*, 11304.

(16) Iversen, B. B.; Larsen, F. K.; Reynolds, P. A.; Figgis, B. N. *Acta Chem. Scand.* **1994**, *48*, 800.
(17) Rauw, W.; Ahsbahs, H.; Hitchman, M. A.; Lukin, S.; Reinen, D.; Schultz, A. J.; Simmons, C. J.; Stratemeier, H. *Inorg. Chem.* **1996**, *35*, 1902.
(18) Bebendorf, J.; Bürgi, H.-B.; Gamp, E.; Hitchman, M. A.; Murphy, A.; Reinen, D.; Riley, M. J.; Stratemeier, H. *Inorg. Chem.* **1996**, *35*, 7419.
(19) Riley, M. J.; Hitchman, M. A.; Reinen, D. *Chem. Phys.* **1986**, *102*, 11.
(20) Rainen, D.; Atanasov, M. *Magn. Reson. Rev.* **1991**, *15*, 167. Rainen, D.; Friebel, C. *Struct. Bonding* **1979**, *37*, 1. Bersuker, I. B.; Polinger, V. Z. *Vibronic Interactions in Molecules and Crystals*; Springer-Verlag: Berlin, 1989.
(21) Misra, S. K.; Wang, C. *Phys. Rev. B* **1990**, *41*, 1.
(22) Reinen, D. *J. Solid State Chem.* **1979**, *27*, 71.
(23) Natsume, Y.; Yamada, I. *Solid State Commun.* **1983**, *47*, 839.
(24) Walsh W. M.; Birgeneau, R. J.; Rupp, L. W.; Guggenheim, H. J. *Phys. Rev. B* **1979**, *20*, 4645.
(25) Maslen E. N.; Ridout S. C.; Watson K. J.; Moore F. H. *Acta Crystallogr.* **1988,** *C44*, 409.
(26) Gill, J. C. *Proc. Phys. Soc., London* **1965**, *85*, 119. de Vroomen, A. C.; Lijphart, E. I.; Poulis, N. J. *Physica* **1970**, *47*, 458.
(27) Gill, J. C. *J. Phys. C: Solid State Phys.* **1975**, *8*, 4203.
(28) Sierra, G. A.; Schweiger, A.; Ernst, R. R. *Chem Phys. Lett.* **1991**, *184*, 363.
(29) Dang, L. S.; Buisson, R.; Williams, F. I. B. *J. Phys.* **1974**, *35*, 49.
(30) Lowrey, M. R.; Pilbrow, J. R. *J. Phys. C: Solid State Phys.* **1977**, *10*, 439.
(31) Rao, P. L.; Viswanath, A. K.; Subramanian, S. *Spectrochim. Acta* **1992**, *48A*, 1745.
(32) Sturge, M. D. *Solid State Physics*, Academic Press: New York, 1967; Vol. 20, p 91.
(33) Williams, F. I. B.; Krupka, D. C.; Breen, D. P. *Phys. Rev.* **1969**, *179*, 255.
(34) Englman, R. *The Jahn−Teller Effect in Molecules and Crystals*; Wiley: London, 1972; chapter 6.
(35) Ham, F. S. *Electron Paramagnetic Resonance*; Plenum Press: New York, 1972; p 1.
(36) Jesion, A.; Shing, Y. H.; Walsh, D. *Phys. Rev. B* **1977**, *16*, 3012.
(37) Breen, D. P.; Krupka, D. C.; Williams, F. I. B. *Phys. Rev.* **1969**, *179*, 241.
(38) Ronning, A. T.; Svare, I. *Phys. Scr.* **1976**, *14*, 79.
(39) Lee, K. P.; Walsh, D. *Phys. Lett.* **1968**, *27A*, 17.
(40) Sussmann, J. A. *J. Phys. Chem. Solids* **1967**, *28*, 1643.
(41) Hoffmann, S. K.; Hilczer, W.; Goslar, J. *J. Magn. Reson. A* **1996**, *122*, 37.
(42) Aminov, L. K.; Kirmse, R.; Solovev, B. V. *Phys. Status Solidi B* **1976**, *77*, 505.
(43) Korradi, G.; Polgar, K.; Vikhnin, V. S.; Dovchenko, L. G.; Zaritskii, I. M. *Fiz. Tverd. Tela* **1984**, *26*, 252.
(44) Hoffmann, S. K.; Hilczer, W.; Goslar, J.; Augustyniak, M. A.; Gramza, M.; Morawski, P. *Mol. Phys. Rep.* **1997**, *18/19*, 51.
(45) Tsvetkov, Yu. D.; Dzuba, S. A. *Appl. Magn. Reson.* **1990**, *1*, 179.
(46) Hoffmann, S. K.; Hilczer, W.; Goslar, J. *Solid State Commun.* **1996**, *100*, 449.
(47) Zimpel, Z. *J. Magn Reson.* **1989**, *85*, 314.